# Polarity governs atomic interaction through two-dimensional materials

Wei Kong[1,11], Huashan Li[3,2,11], Kuan Qiao[1,11], Yunjo Kim[1], Kyusang Lee[1,4], Yifan Nie[5], Doyoon Lee[1], Tom Osadchy[6], Richard J Molnar[6], D. Kurt Gaskill[7], Rachael L. Myers-Ward[7], Kevin M. Daniels[7], Yuewei Zhang[8], Suresh Sundram[9], Yang Yu[2], Sang-hoon Bae[1], Siddharth Rajan[8], Yang Shao-Horn[2], Kyeongjae Cho[5], Abdallah Ougazzaden[9], Jeffrey C. Grossman[2]* and Jeehwan Kim[1,2,10]*

**The transparency of two-dimensional (2D) materials to intermolecular interactions of crystalline materials has been an unresolved topic. Here we report that remote atomic interaction through 2D materials is governed by the binding nature, that is, the polarity of atomic bonds, both in the underlying substrates and in 2D material interlayers. Although the potential field from covalent-bonded materials is screened by a monolayer of graphene, that from ionic-bonded materials is strong enough to penetrate through a few layers of graphene. Such field penetration is substantially attenuated by 2D hexagonal boron nitride, which itself has polarization in its atomic bonds. Based on the control of transparency, modulated by the nature of materials as well as interlayer thickness, various types of single-crystalline materials across the periodic table can be epitaxially grown on 2D material-coated substrates. The epitaxial films can subsequently be released as free-standing membranes, which provides unique opportunities for the heterointegration of arbitrary single-crystalline thin films in functional applications.**

I t is well-known that the in-plane $sp^2$ bonding of graphene stabilizes its single-atom-thick structure[1,2], whereas out-of-plane van der Waals bonding leads to a weak interplanar interaction[3–5]. The transparency of graphene to atomic interactions at such narrow spacing has been of great interest[6–14]. The first evidence was reported by demonstrating the dependence of water droplet wetting angles on graphene with varying supporting substrates[13]. However, contradictory experimental results were also reported[15–19], in which water droplets maintained the same wetting angle regardless of the graphene thickness and underlying substrates. Later, the classic theory of van der Waals interaction along with molecular dynamics simulation were used to approximate the wettability of graphene, which led to the conclusion that monolayer (1 ML) graphene can transmit 30% of the water–substrate interaction[20]. Nevertheless, measuring the wetting angles of water droplets may not be the most precise approach to investigate the transparency of graphene to atomic interaction. The contact area of a water droplet is at the scale of hundreds of square micrometres with trillions of atoms engaged to graphene, and contaminants[15], roughness[16], doping[19,21,22] and defects of graphene can interfere with the shape of a macro-droplet[17,18,23,24]. Thus, water droplet studies on other atomically thin two-dimensional (2D) materials, such as hexagonal boron nitride (hBN), molybdenum disulfide ($MoS_2$) and tungsten disulfide ($WS_2$), have not been conclusive so far[23–27]. More recently, atomic interaction transmitted through 1 ML graphene has been experimentally confirmed by the epitaxial growth of GaAs on monolayer-graphene-coated GaAs substrates, and an epitaxial alignment of Ga atoms to As atoms through 1 ML graphene was found[9]. Although

this work provides the opportunity to study remote atomic interactions through 2D materials, the exact mechanisms of atomic interactions transmitted through 2D materials in general and the impacts of bonding chemistry of substrate materials and 2D materials remain unclear.

In this work, we report general rules for the remote atomic interaction of underlying substrates with overlaying films through 2D materials, dictated by atomic bonding characters of the involved material systems. The insights were gleaned from experimental observations of the remote interaction for various materials. First, to verify if remote atomic interaction through graphene is universal for all crystalline materials, we performed epitaxial growths of GaN, Si and Ge on monolayer-graphene-coated GaN(0001), Si(001) and Ge(001) substrates, respectively. The crystallinity of GaN grown on the monolayer-graphene-coated GaN substrate was examined to verify if GaN epilayers read the crystalline registry of the underlying substrates through graphene. As shown in Fig. 1a, electron backscatter diffraction (EBSD) map confirmed an (0001) wurtzite single-crystalline structure across the GaN epilayer. The high-resolution X-ray diffraction (HRXRD) $\omega$–$2\theta$ scan on the GaN epilayer exfoliated from the 1 ML graphene/GaN substrate shows that the out-of-plane crystal orientation of the GaN epilayer fully aligned with the substrate, with the [0001] direction parallel to the surface normal (Supplementary Fig. 1a). The HRXRD $\phi$ scan further shows the in-plane alignment of the GaN epilayer with the underlying GaN substrate through 1 ML graphene (Supplementary Fig. 1b). Thus, this set of experiments leads to the conclusion that the atomic interaction between the GaN epilayer and the substrate successfully

[1]Department of Mechanical Engineering, Massachusetts Institute of Technology, Cambridge, MA, USA. [2]Department of Materials Science and Engineering, Massachusetts Institute of Technology, Cambridge, MA, USA. [3]Sino-French Institute for Nuclear Energy and Technology, Sun Yat-Sen University, Guangzhou, China. [4]Departments of Electrical and Computer Engineering & Materials Science and Engineering, University of Virginia, Charlottesville, VA, USA. [5]Department of Materials Science and Engineering, The University of Texas at Dallas, Richardson, TX, USA. [6]MIT Lincoln Laboratory, Lexington, MA, USA. [7]US Naval Research Laboratory, Washington, DC, USA. [8]Department of Electrical and Computer Engineering, The Ohio State University, Columbus, OH, USA. [9]School of Electrical and Computer Engineering, Georgia Institute of Technology, GT-Lorraine, UMI 2958 Georgia Tech-CNRS, Metz, France. [10]Research Laboratory of Electronics, Massachusetts Institute of Technology, Cambridge, MA, USA. [11]These authors contributed equally: Wei Kong, Huashan Li, Kuan Qiao. *e-mail: jcg@mit.edu; jeehwan@mit.edu
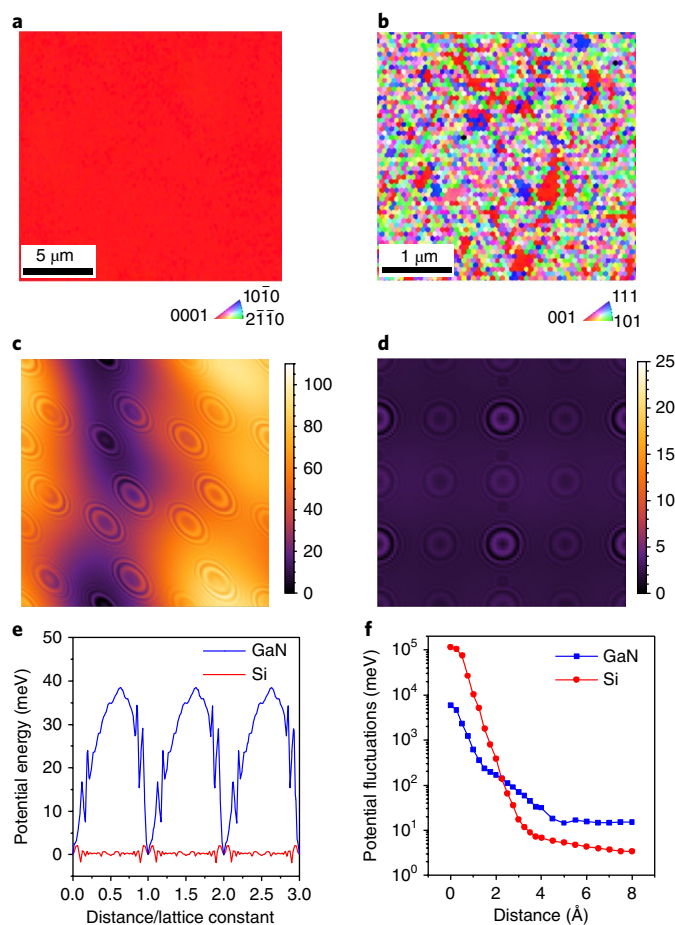
**Fig. 1 | The remote atomic interaction of GaN and Si through 1 ML graphene. a,b**, EBSD of the exfoliated surfaces of GaN (**a**) and Si (**b**). **c,d**, DFT simulations of a potential fluctuation (meV) map at the epitaxial surface of 1-ML-graphene/GaN (**c**) and of 1-ML-graphene/Si (**d**). **e,f**, DFT simulations of the potential fluctuation at the epitaxial surface from GaN and Si through 1 ML graphene (**e**) and of the potential fluctuation decay from the GaN and Si surface (**f**).

fluctuation'—the difference between potential energy maxima and minima along the surface of the substrate—as this fluctuation determines whether incoming adatoms on the surface follow the atomic patterns of the substrates. As shown in Fig. 1c,d, our calculation clearly indicates the different magnitude of electrostatic potential fluctuation transmitted from the Si and GaN substrates through 1 ML graphene. The potential fluctuation from the GaN substrate is well transmitted through 1 ML graphene, and the electrostatic interaction with the GaN substrate is maintained at the epitaxial surface. However, the Si substrate barely preserves its potential fluctuation on the graphene surface. Figure 1e shows a quantitative comparison of the potential energy fluctuation extrapolated from 1-ML-graphene/GaN (Fig. 1c) and 1-ML-graphene/Si (Fig. 1d) surface. The amount of effective potential energy fluctuation (Supplementary Fig. 3) on the epitaxial surface of the 1-ML-graphene/GaN substrates is an order of magnitude higher than that of the 1-ML-graphene/Si substrates (Fig. 1b). Thus, N atoms that arrive on the surface of the 1-ML-graphene/GaN substrates can be stabilized at energetically favourable potential minima, whereas it is more challenging for Si atoms to follow the epitaxial registry from the substrate due to the substantial attenuation of the potential fluctuation from the Si substrate. So far, only the influence of the substrate has been involved, yet the epitaxial relation also depends on the potential profile matching between the epilayer and substrate. To explore the impact of potential profile matching on determining the configuration of the initial nuclei, we considered the accumulated potential energy fluctuation during the growth of nuclei. As shown in Supplementary Figs. 4 and 5, the interaction of GaN nuclei with the GaN substrates beneath graphene increases with the size of the nuclei owing to the accumulation of potential energy fluctuation, allowed by lattice matching between the nuclei and substrates. In contrast, for lattice mismatched system, such as GaN–GaAs, nuclei–substrate interaction does not increase with the size of nuclei. A quantitative comparison of the nuclei–substrate interaction among these three systems is plotted in Supplementary Fig. 6. However, the nuclei–substrate interaction of Si remains negligible even with lattices matching across graphene, owing to the rapid decay of the potential fluctuation. As shown in Fig. 1f, the potential fluctuation from Si decays faster away from the substrate surface compared to that of GaN, and it is significantly lower at the distance defined by monolayer graphene (7 Å for Si and 4.6 Å for GaN). The faster decay of potential fluctuation from Si is due to the pure covalent nature of Si–Si bonding ($r^{-6}$ decay for the Lennard–Jones potential for interaction between neutral systems), whereas the dipole field stemming from the Ga–N ionic bonding follows $r^{-2}$ decay[31].

We further investigated the penetration distance of the electrostatic potential from substrates and its relationship with the ionicity of substrates. We compared the remote interaction penetration of Si, GaAs, GaN and LiF, which possess increasing ionic bonding characters of 0%, 31%, 50% and 90% (refs [28–30,32,33]), respectively. With DFT, we calculated the electrostatic potential fluctuation transmitted from Si, GaAs, GaN and LiF substrates through 1 ML–3 ML graphene based on the atomic models in Fig. 2a (Supplementary Fig. 7). As discussed above, the electrostatic potential fluctuation of the Si substrates through 1 ML graphene is negligible (Fig. 2b1). The same calculation method was used to probe the potential transmission of the GaAs substrates (31% ionicity), where Ga–As form their bonding with a partial ionicity. As shown in Fig. 2b2, the penetration of the potential fluctuation in GaAs substrates through 1 ML graphene is clearly visible and the fluctuation patterns are well maintained. However, 2 ML graphene effectively screens the field from the GaAs substrate, because the potential fluctuation is severely dampened by the increased distance (Fig. 2b3). The potential fluctuation of the GaN substrate, whose fraction of ionic character of 50% is even higher than that of GaAs (refs [28–30,32,33]) can effectively penetrate through 2 ML graphene, but it is significantly dampened by 3 ML

penetrated through 1 ML graphene and guided the atomic alignment of GaN adatoms to the substrate. In contrast, the growth of Si and Ge on monolayer-graphene-coated Si and Ge substrates, respectively, resulted in the formation of polycrystalline Si and Ge. The EBSD map in Fig. 1b taken from Si grown on 1-ML-graphene/Si shows no crystalline order, and a similar polycrystalline EBSD pattern was observed for Ge grown on 1-ML-graphene/Ge (Supplementary Fig. 2 gives the direct homoepitaxy as comparison). This finding suggests that the Si–Si and Ge–Ge atomic interactions are not transmitted through 1 ML graphene, and thus indicate that a remote atomic interaction is not always guaranteed through 1 ML graphene. Given that the bonding characters of Si and Ge are purely covalent, whereas that of GaN is partially ionic, we hypothesized that the atomic bonding characters of materials determine the field penetration through graphene[28–30].

We performed the density functional theory (DFT) calculations (Supplementary Information) to estimate how the arriving atoms interact with the underlying substrate depending on the substrate materials. Our calculations scanned the electrostatic potential distribution contributed by the substrate atoms on the surface directly above graphene, with a distance determined by van der Waals gaps between the arriving atoms and graphene. With the mapping of the electrostatic potential distribution, we aimed to investigate 'potential
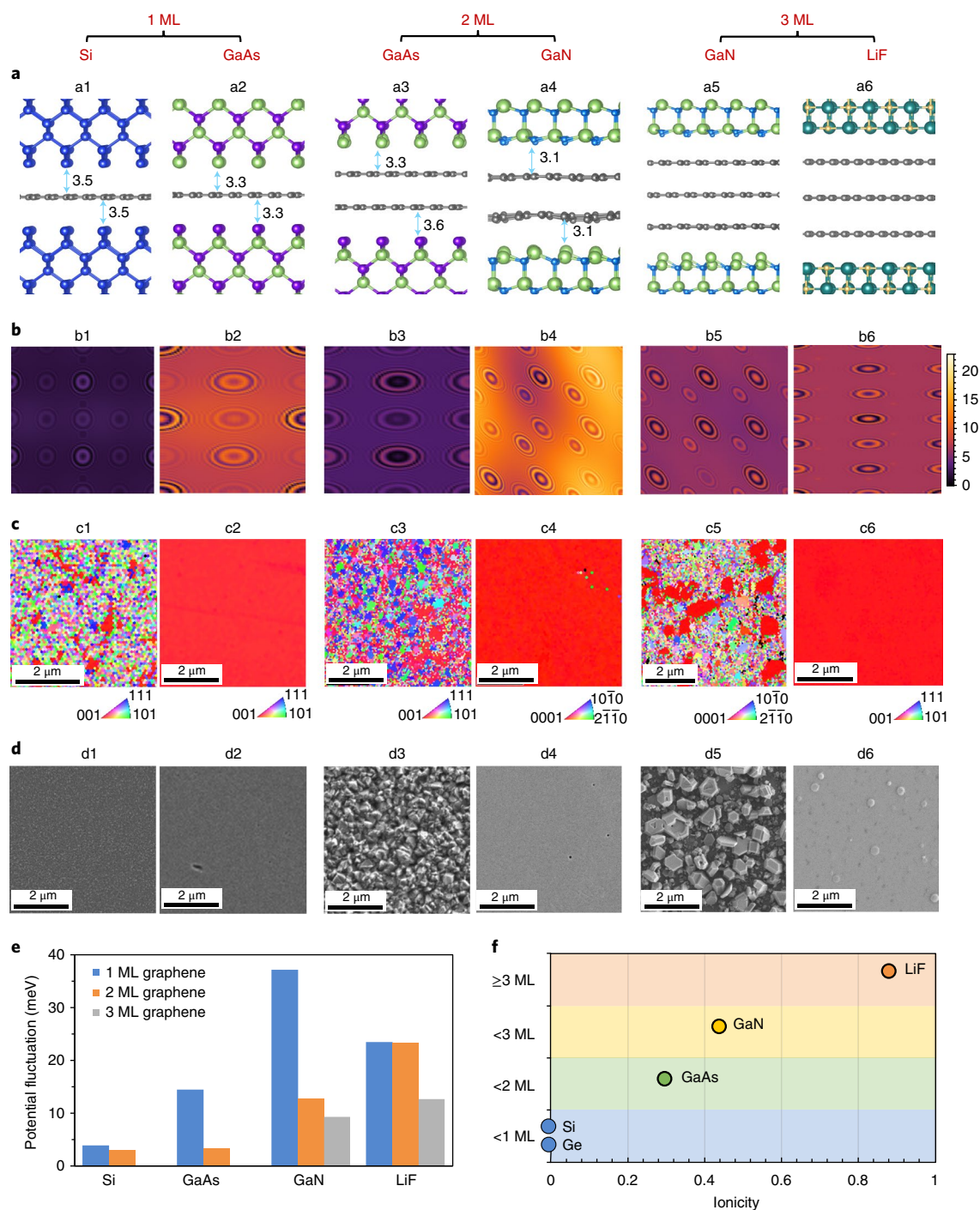
**Fig. 2 | Penetration distance of the potential fluctuations from the Si, GaAs and GaN substrates. a**, DFT-modelled atomic structures of Si, GaAs, GaN and LiF on 1-ML-, 2-ML (bilayer)- or 3-ML (trilayer)-graphene-coated Si, GaAs, GaN and LiF, respectively. C, grey; Si, dark blue; Ga, light green; As, purple; N, blue; Li, dark green; F, orange. **b**, Maps of potential fluctuation on the same scale (0–25 meV) for cross comparison, **c**, EBSD of released surfaces. **d**, Scanning electron microscopy morphology of as-grown surfaces. Within the same column of **a**–**d**, the atomic structure remains identical, being Si/1-ML-graphene (Gr)/Si for (**a1**), (**b1**), (**c1**) and (**d1**), GaAs/1-ML-Gr/GaAs for (**a2**), (**b2**), (**c2**) and (**d2**), GaAs/2-ML-Gr/GaAs for (**a3**), (**b3**), (**c3**) and (**d3**), GaN/2-ML-Gr/GaN for (**a4**), (**b4**), (**c4**) and (**d4**), GaN/3-ML-Gr/GaN for (**a5**), (**b5**), (**c5**) and (**d5**) and LiF/3-ML-Gr/LiF for (**a6**), (**b6**), (**c6**) and (**d6**). **e**, Comparison of the effective potential energy fluctuation on 1-ML-, 2-ML- and 3-ML-graphene-coated substrates. **f**. The schematic of the remote interaction penetration depth depending on ionicity across groups IV, III–V and I–VII materials shows that graphene transparency increases with material ionicity.

graphene, as shown in Fig. 2b4,b5. Even through 3 ML graphene, LiF (with the highest ionic character of 90%) shows a moderate fluctuation and clear atomic patterns, as shown in Fig. 2b6. Thus, our simulations suggest that a strong ionicity in 3D materials allows for the transmission of atomic potential fluctuation beyond the 3 ML graphene gap distance. Figure 2e quantitatively summarizes the potential fluctuation penetration of the Si, GaAs, GaN and LiF substrates as a function of distance (number of graphene layers), and

clearly shows the enhanced penetration of the electrostatic potential from the substrates through graphene by increasing ionic bond characters (Supplementary Fig. 8 explains why the field penetration through 1 ML graphene for GaN is stronger than that for LiF).

To validate our theoretical prediction, we performed the epitaxy of Si, GaAs, GaN and LiF on their own substrates with various thicknesses of the graphene interlayer. The crystallinity of the epitaxial layers is characterized by out-of-plane EBSD mapping of the released surface after exfoliation (Methods describes the exfoliation process)[9,34]. Figure 2c shows that the experimental results have a trend consistent with our theoretical calculations: (1) the growth of Si, which is not guided by the substrate with any number of graphene layers, results in a polycrystalline formation, (2) single-crystalline GaAs is obtained only on 1 ML graphene and not on 2 ML graphene, (3) single-crystalline GaN is obtained with a 2 ML graphene interlayer but not with 3 ML graphene and (4) single-crystalline LiF is obtained even with a 3 ML graphene interlayer. The surface morphologies of Si, GaAs, GaN and LiF grown on 1 ML–3 ML graphene are shown in Fig. 2d. Polycrystalline Si, GaAs and GaN films show rough faceted surface morphologies, whereas single-crystalline GaAs, GaN and LiF films show specular surfaces. Figure 2f summarizes our theoretical and experimental investigation on the critical gap for remote interaction and its relationship to the ionicity of materials. Note that our DFT calculation considers the ground states of epilayer–substrate interaction, and thus the estimation is relevant only when the crystal growth process is not impeded by kinetic barriers. We performed epitaxial growth at the conditions comparable to those of conventional homoepitaxy, which produces high-quality single crystals for the respective material (Methods). In such cases, the registry of the adatoms is determined by the epilayer–substrate interactions (as the choice of substrate). Thus, our experimental trends can be estimated well by DFT (Supplementary Information gives further discussions about the kinetic process of epitaxy on graphene-coated substrates). In addition, kinetic Monte Carlo (KMC) simulation, based on the potential fluctuation values obtained by our DFT calculation, was carried out to estimate the dynamic process of adatoms on graphene-coated substrates. KMC also confirmed that the adatoms on graphene are registered to the underlying substrates (Supplementary Fig. 9).

We note that atomically aligned group IV elemental semiconductors can be obtained, by 'conducting' the remote atomic interaction using a lattice-matched polar interlayer (Supplementary Fig. 10). All group IV, III–V, III–N and I–VII materials on graphene considered here are successfully exfoliated from their substrates, which will provide the freedom for the design of heterogeneous structures that are inaccessible to conventional material synthesis processes, enabling novel functionalities[9,35–38].

The effect of substrate polarity on the field transparency of 2D materials has been well proven through non-polar graphene interlayers. However, field penetrability through polar 2D materials must also be studied because 2D materials that contain ionic bonding characters may interact strongly with the atoms arriving on their surfaces and yield a reduced transparency to the substrate potential field. This hypothesis is proven by our DFT calculation of binding energy fluctuations of the nuclei on polar/non-polar 2D materials, as well as by substrate potential field penetration through these polar 2D materials. In the DFT calculation, we examined the influence of graphene (non-polar) and hBN (polar) on the atomic arrangement of GaN by calculating the binding energy fluctuation of GaN nuclei on the surface of graphene and hBN, respectively. First, we explored a wide range of interfacial configurations of the GaN nuclei on graphene and hBN (Supplementary Figs. 11 and 12), with the high symmetry configurations of maximum and minimum energies shown in Fig. 3a,b. By projecting the binding energy variation on the horizontal coordinate, we estimated the binding energy fluctuation of the GaN nuclei on the surface of graphene and hBN,
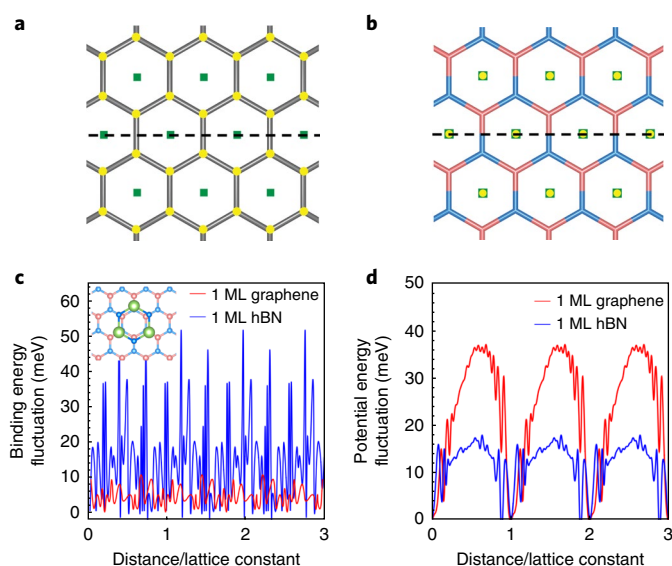


**Fig. 3 | The comparison of energy fluctuation from 2D interlayers (graphene and hBN) and substrates (GaN) for graphene-coated and hBN-coated GaN substrates. a,b,** Binding grids of GaN nuclei on a graphene surface (**a**) and a hBN (**b**) surface with the maximum (yellow) and minimum (green) binding energies. **c,** Binding energy fluctuation from the graphene and hBN surfaces along the black dotted lines shown in **a** and **b**. **d,** Potential energy fluctuation from the GaN substrate through 1 ML graphene and hBN. In **c** and **d**, the unitless quantity 'distance/lattice constant', defined as the ratio of distance along the selected direction to the GaN substrate lattice constant, is introduced to cross compare the energy fluctuation.

as shown in Fig. 3c. The binding energy fluctuation of GaN on hBN increases by fivefold in comparison to that on graphene. Such a strong binding energy fluctuation for GaN nuclei allows 3 nm thick epitaxial hBN (sufficiently away from the substrate field) to seed the growth of single-crystalline GaN (Supplementary Fig. 13)[39,40], whereas thick epitaxial graphene failed to host single-crystalline GaN, as shown in Fig. 2d5. Therefore, such a strong interaction between polar 2D materials and adatoms affects the transparency to the substrate field. As shown in Fig. 3d, our DFT calculation reveals that the substrate potential fluctuation is attenuated by more than a half through 1 ML hBN than that through 1 ML graphene.

To investigate experimentally the field transparency of hBN compared to that of graphene, we performed the epitaxy of GaN on GaN substrates coated with 1 ML, 2 ML and 3 ML epitaxial hBN. The results do not show a complete transmission of the GaN substrate field through 1 ML hBN, because 1 ML hBN partially screens the substrate field, as predicted, and the field is completely screened by 3 ML hBN. As shown in Fig. 4a, the HRXRD ($01\bar{1}6$) in-plane $\phi$ scan of the GaN epilayer on 1-ML-hBN/GaN has two sets of six-fold symmetric diffraction with a 7° azimuthal misalignment from each other. In addition, the in-plane EBSD scans of the GaN epilayer exfoliated from 1-ML-hBN/GaN substrates visualize the intermixing of the two azimuthal crystalline orientations (Fig. 4b), which suggests the coexistence of two different crystalline orientations within the same GaN epitaxial layer. Therefore, this proves that 1 ML hBN is partially transparent to a remote interaction so that the GaN epilayer is seeded from both the hBN and GaN substrates, with remote epitaxy and van der Waals epitaxy both in play. The seeding effect from the substrate is reduced for 2 ML hBN (Fig. 4c) and a complete transition from remote epitaxy to van der Waals epitaxy occurs for 3 ML hBN[4,9], as the substrate potential field is entirely screened by 3 ML hBN to show a single in-plane orientation in the EBSD map
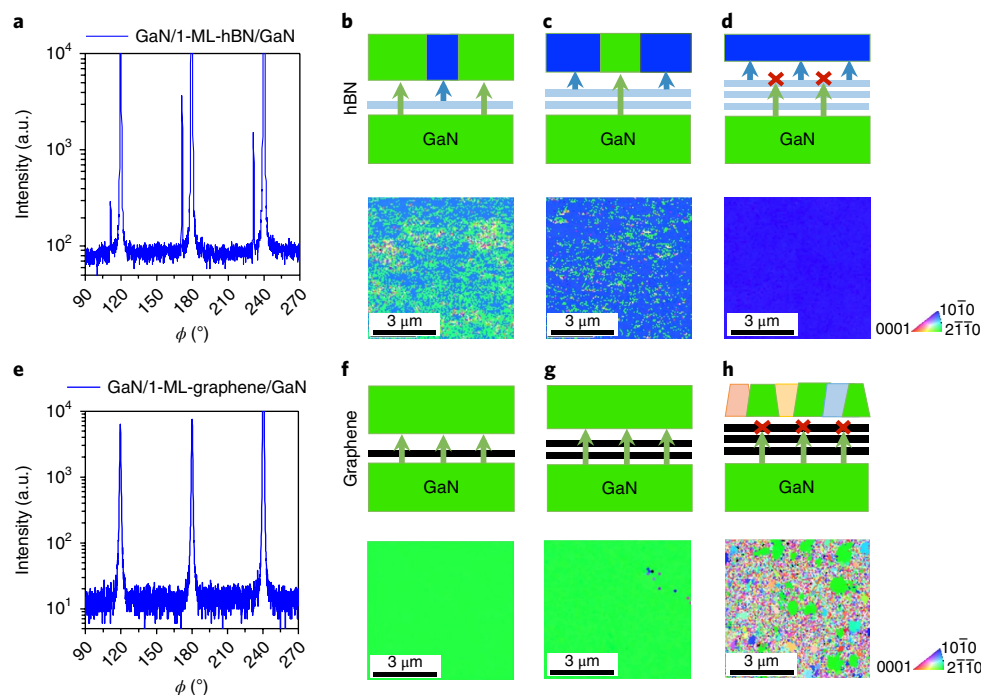
**Fig. 4 | Comparison of the transparency and seeding properties of hBN and graphene. a**, The HRXRD (01$\bar{1}$6) $\phi$ scan of GaN/1-ML-hBN/GaN shows two sets of crystal orientation. **b–d**, Schematic (top) and EBSD (bottom) of the exfoliated surface of GaN on 1-ML-hBN/GaN (**b**), 2ML-hBN/GaN (**c**) and 3ML-hBN/GaN (**d**). **e**, The HRXRD (01$\bar{1}$6) $\phi$ scan of GaN/1-ML-graphene/GaN shows one set of crystal orientation. **f–h**, Schematic (top) and EBSD (bottom) of the exfoliated surface of GaN on 1-ML-graphene/GaN (**f**), 2ML-graphene/GaN (**g**) and 3ML-graphene/GaN (**h**). a.u., arbitrary units.

(Fig. 4d). This makes a clear contrast to the case for graphene. The in-plane HRXRD (01$\bar{1}$6) $\phi$ scan (Fig. 4e) of GaN on the monolayer-graphene-coated GaN substrate shows only one set of six-fold symmetric diffraction, which suggests seeding solely from the GaN substrate. A single colour in the in-plane EBSD maps (Fig. 4f,g) indicates no azimuthal intermixing of orientation with 1 ML and 2 ML graphene interlayers, which confirms graphene's transparency to the GaN potential field. A trilayer graphene interlayer leads to the formation of a polycrystalline film (Fig. 4h), in which seeding from graphene is weak. The experiment and calculation results clearly indicate that 2D materials with polar bonding can screen the field from the substrate due to their increased inhomogeneity of potential distribution, and thus the field transparency for polar 2D materials is less than that of graphene. Based on the results obtained from hBN interlayers, it can be deduced that other polar 2D materials, such as $MoS_2$ and $WS_2$, will screen the field from the substrate because of its three-atom thickness together with polarization in their bonding (Supplementary Figs. 14 and 15 give further simulations of the transition metal dichalcogenides).

In conclusion, we have demonstrated that the polarities of both bulk and 2D materials play a crucial role in determining the transparency of 2D materials to remote atomic interaction. With the very good agreement between simulations and experimental data, our study elucidates general rules for remote interaction through 2D materials: (1) remote atomic interaction penetrates further for strong polarized bulk materials, (2) polarity in 2D materials with an enhanced binding to adatoms reduces the transparency to atomic interaction and (3) the strength of the remote interaction can be controlled by modulating the polarity of the substrate materials as well as the 2D material interlayers. Such an understanding provides unprecedented opportunities for the heterointegration of arbitrary thin-film materials across the periodic table with vastly different properties or crystal orientations onto one substrate. Single-crystalline thin films can be synthesized on 2D-material-coated substrates and subsequently exfoliated to form the elements for heterointegration. As examples, we have shown the exfoliated freestanding and flexible single-crystalline thin films in groups I–VII, III–V and IV materials (Supplementary Fig. 16). In addition, we demonstrated the heterointegration of two crystal orientations on one substrate by modulating remote epitaxy and van der Waals epitaxy.

## Online content

Any methods, additional references, Nature Research reporting summaries, source data, statements of data availability and associated accession codes are available at https://doi.org/10.1038/s41563-018-0176-4.

## References

1. Van den Brink, J. Graphene: from strength to strength. *Nat. Nanotech.* **2**, 199–201 (2007).
2. Lee, C., Wei, X., Kysar, J. W. & Hone, J. Measurement of the elastic properties and intrinsic strength of monolayer graphene. *Science* **321**, 385–388 (2008).
3. Charlier, J.-C., Gonze, X. & Michenaud, J.-P. Graphite interplanar bonding: electronic delocalization and van der Waals interaction. *Europhys. Lett.* **28**, 403–408 (1994).
4. Koma, A. Van der Waals epitaxy—a new epitaxial growth method for a highly lattice-mismatched system. *Thin Solid Films* **216**, 72–76 (1992).
5. Spanu, L., Sorella, S. & Galli, G. Nature and strength of interlayer binding in graphite. *Phys. Rev. Lett.* **103**, 196401 (2009).
6. Shih, C.-J. et al. Breakdown in the wetting transparency of graphene. *Phys. Rev. Lett.* **109**, 176101 (2012).
7. Chae, S. et al. Lattice transparency of graphene. *Nano Lett.* **17**, 1711–1718 (2017).
8. Ramos-Alvarado, B., Kumar, S. & Peterson, G. On the wettability transparency of graphene-coated silicon surfaces. *J. Chem. Phys.* **144**, 014701 (2016).
9. Kim, Y. et al. Remote epitaxy through graphene enables two-dimensional material-based layer transfer. *Nature* **544**, 340–343 (2017).

10. Parobek, D. & Liu, H. Wettability of graphene. *2D Mater.* **2**, 032001 (2015).
11. Ramos-Alvarado, B., Kumar, S. & Peterson, G. Wettability of graphitic-carbon and silicon surfaces: MD modeling and theoretical analysis. *J. Chem. Phys.* **143**, 044703 (2015).
12. Ondarçuhu, T. et al. Wettability of partially suspended graphene. *Sci. Rep.* **6**, 24237 (2016).
13. Rafiee, J. et al. Wetting transparency of graphene. *Nat. Mater.* **11**, 217–222 (2012).
14. Taherian, F., Marcon, V., van der Vegt, N. F. & Leroy, F. What is the contact angle of water on graphene? *Langmuir* **29**, 1457–1465 (2013).
15. Li, Z. et al. Effect of airborne contaminants on the wettability of supported graphene and graphite. *Nat. Mater.* **12**, 925 (2013).
16. Singh, E. et al. Graphene drape minimizes the pinning and hysteresis of water drops on nanotextured rough surfaces. *ACS Nano* **7**, 3512–3521 (2013).
17. Raj, R., Maroo, S. C. & Wang, E. N. Wettability of graphene. *Nano Lett.* **13**, 1509–1515 (2013).
18. Shin, Y. et al. Surface-energy engineering of graphene. *Langmuir* **26**, 3798–3802 (2010).
19. Hong, G. et al. On the mechanism of hydrophilicity of graphene. *Nano Lett.* **16**, 4447–4453 (2016).
20. Shih, C.-J., Strano, M. S. & Blankschtein, D. Wetting translucency of graphene. *Nat. Mater.* **12**, 866–869 (2013).
21. Li, X. et al. Influence of water on the electronic structure of metal-supported graphene: insights from van der Waals density functional theory. *Phys. Rev. B* **85**, 085425 (2012).
22. Zhang, L. et al. Janus graphene from asymmetric two-dimensional chemistry. *Nat. Commun.* **4**, 1443 (2013).
23. Lee, C. H., Drelich, J. & Yap, Y. K. Superhydrophobicity of boron nitride nanotubes grown on silicon substrates. *Langmuir* **25**, 4853–4860 (2009).
24. Li, H. & Zeng, X. C. Wetting and interfacial properties of water nanodroplets in contact with graphene and monolayer boron–nitride sheets. *ACS Nano* **6**, 2401–2409 (2012).
25. Gaur, A. P. et al. Surface energy engineering for tunable wettability through controlled synthesis of $MoS_2$. *Nano Lett.* **14**, 4314–4321 (2014).
26. Chow, P. K. et al. Wetting of mono and few-layered $WS_2$ and $MoS_2$ films supported on $Si/SiO_2$ substrates. *ACS Nano* **9**, 3023–3031 (2015).
27. Kozbial, A., Gong, X., Liu, H. & Li, L. Understanding the intrinsic water wettability of molybdenum disulfide ($MoS_2$). *Langmuir* **31**, 8429–8435 (2015).
28. Christensen, N., Satpathy, S. & Pawlowska, Z. Bonding and ionicity in semiconductors. *Phys. Rev. B* **36**, 1032 (1987).
29. Gordy, W. & Thomas, W. O. Electronegativities of the elements. *J. Chem. Phys.* **24**, 439–444 (1956).
30. Phillips, J. Ionicity of the chemical bond in crystals. *Rev. Modern Phys.* **42**, 317 (1970).
31. Lennard-Jones, J. E. Cohesion. *Proc. Phys. Soc.* **43**, 461 (1931).
32. Catlow, C. & Stoneham, A. Ionicity in solids. *J. Phys. C* **16**, 4321 (1983).
33. Gottschalk, H., Patzer, G. & Alexander, H. Stacking fault energy and ionicity of cubic III–V compounds. *Phys. Status Solidi* **45**, 207–217 (1978).
34. Kim, J. et al. Principle of direct van der Waals epitaxy of single-crystalline films on epitaxial graphene. *Nat. Commun.* **5**, 5836 (2014).
35. Striemer, C. C., Gaborski, T. R., McGrath, J. L. & Fauchet, P. M. Charge- and size-based separation of macromolecules using ultrathin silicon membranes. *Nature* **445**, 749–753 (2007).
36. Lee, D. et al. Emergence of room-temperature ferroelectricity at reduced dimensions. *Science* **349**, 1314–1317 (2015).
37. Yoon, J. et al. Ultrathin silicon solar microcells for semitransparent, mechanically flexible and microconcentrator module designs. *Nat. Mater.* **7**, 907–915 (2008).
38. Ko, H. et al. Ultrathin compound semiconductor on insulator layers for high-performance nanoscale transistors. *Nature* **468**, 286–289 (2010).
39. Ayari, T. et al. Wafer-scale controlled exfoliation of metal organic vapor phase epitaxy grown InGaN/GaN multi quantum well structures using low-tack two-dimensional layered h-BN. *Appl. Phys. Lett.* **108**, 171106 (2016).
40. Li, X. et al. Large-area two-dimensional layered hexagonal boron nitride grown on sapphire by metalorganic vapor phase epitaxy. *Crystal Growth Design* **16**, 3409–3415 (2016).

## Acknowledgements

## Author contributions

J.C., W.K. and K.Q. conceived the experiments. J.C.G., J.K., H.L. and W.K. design theoretical modelling. J.C.G. and H.L. performed the DFT calculation. K.C. and Y.N. performed the KMC simulation. W.K., K.Q., Y.K., K.L., D.L. and S.-H.B. contributed to the 2D material handling, measurements, and synthesis of Si, Ge, GaAs, GaN and LiF, T.O., R.J.M., Y.Z. and S.R. contributed to GaN synthesis, D.K.G., R.L.M.-W. and K.M.D. contributed to the graphene synthesis, S.S. and A.O. contributed to the hBN synthesis and Y.Y. and Y.S.H. contributed to the LiF synthesis. All the authors contributed to the discussions and analysis of the results regarding the manuscript. J.K. directed the team.

## Competing interests

The authors declare no competing interests.

## Additional information

## Methods

**Graphene formation and transfer.** We used epitaxial graphene for the transparency demonstration. We synthesized 1 ML epitaxial graphene by graphitization of a nominally on-axis semi-insulating 4H-SiC (0001) wafer at 1,580 °C in 100 mbar Ar ambient for 20 min in an Aixtron VP508. Before graphitization, the wafer was etched in ultrahigh purity $H_2$. The 1 ML epitaxial graphene was exfoliated using a layer-resolved graphene transfer (LRGT) process. A metal stressor was applied to the 1 ML graphene using a RMV Intelsi-L PVD, and a thermal release tape was used as a mechanical handle to release the graphene from the SiC surface. To ensure the closest contact proximity of graphene to the substrates, native oxide of all substrates was removed by chemical etching treatments, the 1 ML graphene was then immediately transferred onto the treated surface of the target epitaxial substrate[41,42]. The thermal release tape was removed at the release temperature using a hotplate. The metal stressor was dissolved by a chemical etchant. Both 2 ML and 3 ML graphene were formed by repeating the same procedure on a 1 ML and 2 ML, respectively, graphene-coated epitaxial substrate surface. For LiF, the graphene was instead transferred by poly(methylmethacrylate) (PMMA) from a 2 ML or 3 ML graphene-coated $SiO_2$/Si substrate. In this process, PMMA was spin cast on a 2 ML graphene-coated $SiO_2$/Si substrate, and the graphene was released by etching away the $SiO_2$ layer. Using PMMA as a handler, the graphene was transferred onto the LiF substrate surface. The PMMA was subsequently removed by acetone and thermal annealing in a vacuum environment. After transferring, the number of layers and the quality of transferred graphene were confirmed by Raman spectroscopy for all the samples (Supplementary Fig. 17). After the growth, we confirmed that the graphene remains unetched as we observed the successful exfoliation of epitaxial layers from 1 ML graphene.

**hBN formation and transfer.** hBN was epitaxially grown on a two-inch (0001) sapphire substrate, and the growth procedure is described in a report elsewhere[40]. The thickness of the hBN layer was 3 nm. The 3 nm hBN was exfoliated from the sapphire substrate to be a free-standing hBN thin film by using the LRGT process described above. The 1 ML hBN was separated from the 3 nm hBN thin film by using the LRGT process on the exposed surface of the free-standing hBN freshly exfoliated from the sapphire substrate. The separation procedure was published elsewhere. The exfoliated hBN was subsequently transferred or stacked onto the substrate of interest, using the same process as for the graphene transfer described above[41].

**Epitaxial growth.** Epitaxial growth of GaAs, Si and Ge was performed using different metalorganic chemical vapour deposition (MOCVD) reactors for IV and III–V epitaxy. For GaAs, arsine and trimethylgallium were used as the precursors for the As and Ga sources, respectively. During growth, the reactor conditions were set to 650 °C and 100 torr with an input III–V molar ratio of 1:40 using high purity nitrogen as the carrier gas. For Si and Ge epitaxy, silane and germane were used for the Si and Ge sources, respectively. Epitaxial growth was carried out at 650 °C and 100 torr using ultrahigh purity hydrogen as the carrier gas. GaN epitaxial layers of about 0.3–2 μm thick were grown on the graphene or hBN-coated GaN substrate by using both MOCVD and molecular beam epitaxy (MBE). The growth of GaN in an MOCVD reactor occurred at the growth temperature of 1,170 °C, mediated by a thin GaN buffer layer grown at 750 °C to avoid the etching of graphene. Trimethylgallium and high purity ammonia were employed as the reactants, and high purity nitrogen was used as the ambient gas. The GaN growths were carried out using Veeco Gen 930 $N_2$ plasma-assisted MBE system, equipped with a standard effusion cell for Ga, and a Veeco Uni-Bulb $N_2$ plasma source. The GaN growth in MBE occurred at a substrate temperature of 700 °C under slightly Ga-rich conditions, with a radiofrequency plasma power of 250 W. The results from MOCVD and MBE are consistent. LiF was grown by pulsed-laser deposition. LiF powder of 99.995% purity was sintered at 300 °C in high purity Ar ambient for 6 h to form the target. LiF of thickness 300 nm was grown at a substrate temperature of 300 °C in vacuum with a base pressure of $1 \times 10^{-6}$ torr.

**Epitaxial thin film exfoliation.** The epilayers were exfoliated using 50 nm Ti and about 1–5 μm Ni as a stressor. Stress induced by the Ni stressor caused preferential cleaving at the epilayer and substrate interface. The epilayer and substrate separation was handled using a thermal release tape as a mechanical support.

## Data availability

The data that support the findings of this study are available from the corresponding authors on reasonable request.

## References

41. Kim, J. et al. Layer-resolved graphene transfer via engineered strain layers. *Science* **342**, 833–836 (2013).
42. Bae, S.-H. et al. Unveiling the carrier transport mechanism in epitaxial graphene for forming wafer-scale, single-domain graphene. *Proc. Natl Acad. Sci. USA* **114**, 4082–4086 (2017).